Final Draft
of the original manuscript:

Chu, Q.; Li, W.Y.; Yang, X.W.; Shen, J.J.; Li, Y.B.; Wang, W.B.:
Study of process/structure/property relationships in probeless friction stir spot welded AA2198 Al-Li alloy
In: Welding in the World (2017) Springer

DOI: 10.1007/s40194-017-0423-3

Study of process/structure/property relationships in probeless friction stir spot welded AA2198 Al-Li alloy

Q. Chu[1], W.Y. Li[1,*], X.W. Yang[1], J.J. Shen[2], Y.B. Li[3], W.B. Wang[4]

[1]State Key Laboratory of Solidification Processing, Shaanxi Key Laboratory of Friction Welding Technologies, Northwestern Polytechnical University, Xi'an 710072, Shaanxi, PR China

[2]Helmholtz-Zentrum Geesthacht, Institute of Materials Research, Materials Mechanics, Geesthacht 21502, Germany

[3]Shanghai Key Laboratory of Digital Manufacture for Thin-walled Structures, School of Mechanical Engineering, Shanghai Jiao Tong University, Shanghai 200240, PR China

[4]China FSW Center, Beijing 100024, PR China

* Corresponding author. Tel.: ++86-29-88495226, Fax: ++86-29-88492642, E-mail: liwy@nwpu.edu.cn (W.Y. Li)

Abstract: Probeless friction stir spot welding (probeless FSSW) is a useful variant of conventional friction stir spot welding (FSSW), where there is no probe at the end of the tool shoulder. In this study, AA2198-T8 aluminum-lithium alloy has been successfully welded by probeless FSSW. The variations of geometric features of probeless FSSWed joints: stir zone width, stir zone edge angle and hook angle, and their effects on the joint mechanical properties were studied quantitatively. Results show that the width of stir zone is constrained by shoulder diameter, and the ratio of the width to shoulder diameter approaches 0.9. With the increase of stir zone depth, the stir zone edge angle approaches 45 °eventually during the welding process. Additionally, the hook defect can be found among all of the probeless FSSWed joints due to the upward material flow of the lower sheet. When the hook angle is around 90 °, the tensile/shear strength reaches a relatively higher value. The fracture mode changes from shear fracture to plug fracture when hook angle transforms from obtuse to acute.

Keywords: Probeless friction stir spot welding; Macrostructure; Mechanical property; Fracture mechanism

Introduction

In order to reduce the weight and achieve a high performance of the structural components, lightweight materials such as aluminum have been increasingly used in the automotive and aerospace industries [1-3]. However, joining Al-Li alloys by fusion welding is challenging due to the associated solidification defects such as hot cracking and porosity [4, 5]. Friction stir welding (FSW) is an innovative solid-state process which has several advantages over traditional fusion welding, such as uniform microstructure, sound mechanical properties and small thermal deformation. [6-10].

As a variant of FSW, friction stir spot welding (FSSW) shows great potential to be a replacement of single-point joining processes like resistance spot welding and riveting in aluminum alloys [11-13, 17-19]. However, the keyhole defect is the typical feature in FSSWed joints, seriously reducing joint properties. Thus, the refilling FSSW and probeless FSSW were developed to eliminate the keyhole [14-16, 20-23]. Uematsu et al. [16] proved that the tensile strength of the refilling FSSWed joints was enhanced, but the fatigue strength was slightly decreased. Furthermore, the equipment for the refilling FSSW process is extremely complex. Thus, the probeless FSSW process was used to avoid the keyhole, and the joints showed an increased tensile strength compared to the probe FSSWed joints [21].

Investigations of FSSW were mainly focused on microstructure and joint mechanical properties [17, 18], and there has been little work on the relationship between joint geometry (stir zone width, stir zone edge angle and hook angle) and mechanical properties, which is useful for performance prediction and parameters optimization. Yin et al. [19] investigated the influence of dwell time on the macrostructure of FSSWed joints and found that the beneficial effect of increasing bonded width on failure load is outweighed by the detrimental change of hook defect. Rosendo et al. [20] revealed that the fracture modes were associated to the hook sharpness which is strongly related to the dwell time and should be responsible for the deterioration of the joint mechanical strength. Similarly, Tozaki et al. [21] found that the mechanical properties were mainly governed by the geometrical features of joints especially the hook defect (HD). However, the evolution of joint macrostructure was not studied quantitatively, and its effect on mechanical property was not investigated systematically. Moreover, in our previous study, it was found that the stir zone edge angle (SEA) and hook angle (HA), as shown in Fig. 1, which were used to characterize the joint macrostructure, were related to joint mechanical properties [22]. Thus, the main purposes of this study are to investigate the variations of geometrical features of probeless FSSWed joints quantitatively and examine the relationship between macrostructure and mechanical properties.

Experimental procedures

1.8mm thick sheets of 2198-T8 Al-Li alloy (60mm×30mm) were lap-welded by probeless FSSW, which were cleaned with acetone. The chemical composition and mechanical properties are shown in Table 1 and 2. A probeless cylindrical tool with the shoulder diameter (D) of 15mm was used which was made of H13, and three involute grooves were machined on the shoulder surface. To investigate the variation of the joint structure, different parameters were used as shown in Table 3, according to the previous study [22, 23].

The SEA and HA were measured from the cross-section of probeless FSSWed joint. Samples for morphology analysis were etched using the Keller's Reagent (2 ml HF, 3 ml HCl, 5 ml HNO_3, and 190 ml H_2O), and examined by optical microscopy (OM). For the tensile/shear tests, specimens were

produced using two 60mm×30mm coupons with an overlap length of 30mm and the tests were carried out in triplicate for each welding parameter at a head cross speed of 1mm/min by using a testing machine. Then the fracture features of the samples were analyzed by scanning electron microscope (SEM).

Results and discussion

Typical microstructure

Fig. 2 reveals the typical microstructure of the cross-section of probeless FSSWed joint made at the rotation speed of 950 rpm and dwell time of 12s. According to the characteristic of the cross-section which shows an asymmetrical 'basin' shape (Fig. 2a), the cross-section can be divided into three regions: the stir zone (SZ), the thermo-mechanically affected zone (TMAZ) and the heat affected zone (HAZ).

Close-up views of different zones as marked in Fig. 2a show that the region B (Fig. 2b) indicating SZ is characterized by equiaxed grains which can be attributed to dynamic recrystallization. In region C (Fig. 2c), the TMAZ is characterized by highly deformed grains, which undergo severe friction heating and plastic deformation. The microstructure of HAZ was similar to that of base materials (BM), which exhibited typical microstructure parallel to the rolling direction but with coarser grains due to the limited temperature during the welding process. In addition, it can be seen that the boundary (Region D) presents an upside down 'V' shaped appearance for the upward flow of extruded materials of lower sheet. Thus, it forms the hook defect as marked in Fig. 2a, which is the weak connection.

The model of macrostructure

Based on the macroscopic observations, the macrostructure evolution of the probeless FSSWed joint is schematically illustrated in Fig. 3, which consists of two major stages, plunge stage and dwell stage. In the plunge stage, the shoulder moves downward at a constant rotation speed and plunge rate, which is completed in a short time. With the contact and penetration of the shoulder, the temperature at the upper sheet surface increases rapidly for friction heat which is determined by the rotation speed and plunge rate, and small part of softened materials are extruded to form a flash (Fig. 3b) [24-26]. Then, in the dwell stage, the stir zone starts to expand with the increase of dwell time (Fig. 3c-3f). However, the stir zone expands horizontally preferentially for severe deformation and high temperature at the surface during the initial dwell period. Subsequently, the stir zone depth increases rapidly and the upward material flow of the lower sheet occurs markedly [27, 28]. Thus, the interface between two sheets bends upward and extends to the stir zone periphery resulting in the formation of hook defect.

According to the macrostructure of probeless FSSWed joint, a model is established to analysis the variation of the joint morphology. As shown in Fig. 1, the stir zone width (SW, defined as L), the angle of stir zone edge (SEA) and the angle of hook defect (HA) are the significant geometrical parameters

characterizing the joint structure. The changes of these factors with process parameters are detailed below.

Fig. 4 shows the stir zone width as a function of process parameters. It can be seen from Fig. 4a that stir width (L) increases gently with dwell time. With the contact of the shoulder, the temperature at the surface of upper sheet rises rapidly. With the increase of dwell time, the material flow becomes more and more intensely for the sufficient energy input resulting in the increase of L. But the width of stir zone is constrained by shoulder diameter, and the ratio of the width to shoulder diameter (D) approaches 0.9. Additionally, the effects of plunge rate and rotation speed on L are shown in Fig. 4b and Fig. 4c. The change of stir zone width with rotation speed is similar with that of dwell time but the width keep constant substantially with changing the plunge rate. It can be summarized that the dwell time and rotation speed have significant effects on the L/D ratio, while the plunge rate has a slightly effect.

The variations of SEA and HA with process parameters are shown in Fig. 5. With the increase of dwell time, the SEA increases rapidly at the beginning and approximates 45 ° finally (Fig. 5a) while the HA decreases rapidly with dwell time. It can be explained that the material underneath the shoulder softened by friction heat is pushed down and then moves outside to the periphery of stir zone intensely, resulting in the change of SEA. With the increase of SZ depth, the upward material flow of lower sheet occurs markedly. As a result, the boundary between two sheets bends upward and the HA changes from obtuse to acute finally. The similar changes of SEA and HA are observed with increasing rotation speed (Fig. 5c). It should be noted that the HA increases abnormally as more materials are extruded to flash when the rotation speed exceeds 950rpm. In addition, it can be seen that the plunge rate has slight effect on the SEA and HA (Fig. 5b).

Mechanical properties

Tensile/shear strength and fracture mechanism

According to the variations of HA (Fig. 5) and tensile/shear strength (Fig.6), it can be found that the tensile/shear strength shows different trends when HA is obtuse and acute. Thus, HA is replaced by the angular difference between HA and 90 ° (θ) to study its effect on the tensile/shear strength (Fig. 6). It can be seen that the maximum load increases initially and then decrease with the increase of dwell time, while it shows an opposite trend with rotation speed (Fig. 6a and 6c). In addition, Fig. 6a shows that the HA approaches 90 ° and then changes from obtuse ($90<\theta<180$) to acute ($\theta<90$) with the dwell time longer than 6s due to the upward flow of the softened materials in lower sheet caused by the sufficient energy input, but it changes slightly with plunge rate (Fig. 6b). It can be summarized that the dwell time and rotation speed have significant effects on the tensile/shear strength and HA of the probeless FSSWed joints, while the plunge rate has a slightly effect on them. Besides, it can be seen that the

maximum load is significantly affected by HA. When HA is around 90 °, the maximum load reaches a relatively higher value. With the increase of dwell time, HA is obtuse and close to 90 °initially, thus the tensile/shear strength increases due to the increases of SW and SEA. Although the SW and SEA still increase when dwell time exceeds 6s, the HA transforms into acute and gets away from 90 ° accordingly resulting in the decrease of tensile/shear strength. Due to the upward material flow of the lower sheet, the hook defect becomes too sharp, resulting in rapid decrease of the effective thickness of upper sheet. Since the hook defect works as a crack nucleation site, a crack can nucleate and grows in the upper sheet under small loads. Therefore, the joint tensile/shear strength is mainly affected by the SW and SEA when the HA exceeds 90 °but it is governed by the hook defect when HA transforms into acute.

Based on the results of tensile/shear test, two different fracture modes, shear fracture and plug fracture, are observed. Both of the fracture modes are associated to the same fracture mechanism in which the hook defect plays an important role, as schematically illustrated in Fig. 7. As the dwell time increases, the failure location shifts further away from the interface (shear fracture), towards the surface of upper sheet and occurs at the hook defect in the top sheet finally (plug fracture). Since the hook works as a crack nucleation site, when it becomes too sharp, a crack can nucleate and grow on the upper sheet under small loading levels. Fig. 8a shows the shear fracture that occurred under the condition of the rotation speed of 950rpm and dwell time of 6s. It should be noted that elongated dimples are extensively seen in section B (Fig. 8b), indicating good bonding between both sheets. When the dwell time extends from 6s to 15s, the fracture mode transforms from shear fracture to plug fracture (Fig. 8c). It can be seen that there are tearing edges and flat facets in region C (Fig. 8d), indicating that the hook defect is the weak connection zone. Therefore, the hook geometry plays an important role in the fracture mechanism of probeless FSSWed joints, and is responsible for the decrease of the joints strength made at dwell times longer than 6s (Fig. 6a).

Conclusions

The variations of geometric features of probeless FSSWed AA2198 joints and the relationship between the macrostructure and mechanical properties are investigated quantitatively. The following conclusions could be drawn:

(1) Three distinct zones with different microstructures are observed in the cross-section of probeless FSSWed joint: SZ, TMAZ and HAZ. In addition, the width of stir zone is constrained by the shoulder diameter, and the ratio of the width to shoulder diameter approaches 0.9.

(2) The variations of SEA and HA in probeless FSSWed joints are investigated quantitatively. With the increase of dwell time, SEA increases rapidly at first, then approaches 45 °while HA decreases

rapidly since the SZ gradually expands to the depth direction and the upward material flow of the lower sheet occurs markedly.

(3) The tensile/shear strength is significantly affected by HA. When HA is around 90°, the tensile/shear strength reaches a relatively higher value. Two different fracture modes: shear fracture and plug fracture, are observed related to the morphology of hook defect. Since the hook works as a crack nucleation site, when it becomes too sharp, a crack can nucleate and grow on the upper sheet resulting in the transformation from shear fracture into plug fracture.

Acknowledgments

The authors would like to appreciate the financial support from the National Natural Science Foundation of China (515774196), the Open Fund of Shanghai Key Laboratory of Digital Manufacture for Thin-walled Structures (2014003) and the 111 Project (B08040).

References

[1] Badarinarayana H, Yang Q, Zhu S (2009) Effect of tool geometry on static strength of friction stir spot-welded aluminum alloy. Int J Mach Tool Manu 49:142-148

[2] Klobčar D, Tušek J, Smolej A, Simončič S (2015) Parametric study of FSSW of aluminium alloy 5754 using a pinless tool. Weld World 59(2):269-281

[3] Sajed M, Bisadi H (2016) Experimental failure study of friction stir spot welded similar and dissimilar aluminum alloys. Weld World 60(1):33-40

[4] Xiao RS, Zhang XY (2014) Problems and issues in laser beam welding of aluminum-lithium alloys. J Manuf Process 16:166-175

[5] Pakdil M, Çam G, Ko çak M, Erim S (2011) Microstructural and Mechanical Characterization of Laser Beam Welded AA6056 Al-Alloy. Mater Sci Eng A 528:7350-7356

[6] Zhang ZH, Li WY, Feng Y, Li JL, Chao YJ (2015) Global anisotropic response of friction stir welded 2024 aluminum sheets. Acta Mater 92:117-125

[7] Zhang ZH, Li WY, Wang FF, Li JL (2016) Sample geometry and size effects on tensile properties of friction stir welded AA2024 joints. Mater Lett 162:94-96

[8] Zhang Z, Xiao BL, Ma ZY (2015) Enhancing mechanical properties of friction stir welded 2219Al-T6 joints at high welding speed through water cooling and post-welding artificial ageing. Mater Charact 106:255-265

[9] Çam G, İpekoğlu G, Tarık Serindağ H (2014) Effects of use of higher strength interlayer and external cooling on properties of friction stir welded AA6061-T6. Sci Technol Weld Joi 19:715-720

[10] Ji SD, Meng XC, Huang RF, Ma L, Gao SS (2016) Microstructures and mechanical properties

of 7n01-t4 aluminum alloy joints by active-passive filling friction stir repairing. Mater Sci Eng A 664:94-102

[11] Bozkurt Y, Salman S, Cam G (2013) Effect of welding parameters on lap shear tensile properties of dissimilar friction stir spot welded AA 5754-H22/2024-T3 joints. Sci Technol Weld Joi 18:337-345

[12] Yang XW, Fu T, Li WY (2014) Friction stir spot welding: a review on joint macro-and microstructure, property, and process modelling. Adv Mater Sci Eng 2014(1):1-11

[13] Yuan W, Mishra RS, Webb S, Chen YL, Carlson B, Herling DR (2011) Effect of tool design and process parameters on properties of al alloy 6016 friction stir spot welds. J Mater Process Tech 211(6):972-977

[14] Dong HG, Chen S, Song Y, Guo X, Zhang XS, Sun ZY (2016) Refilled friction stir spot welding of aluminum alloy to galvanized steel sheets. Mater Design 94:457-466

[15] Zhao YQ, Liu HJ, Chen SX, Lin Z, Hou JC (2014) Effects of sleeve plunge depth on microstructures and mechanical properties of friction spot welded alclad 7B04-T74 aluminum alloy. Mater Design 62(10):40-46

[16] Uematsu Y, Tokaji K, Tozaki Y, Kurita T, Murata S (2008) Effect of re-filling probe hole on tensile failure and fatigue behaviour of friction stir spot welded joints in Al–Mg–Si alloy. Int J Fatigue 30:1956-1966

[17] Zhang Z, Xiao BL, Ma ZY (2014) Influence of water cooling on microstructure and mechanical properties of friction stir welded 2014Al-T6 joints. Mater Sci Eng A 614(37):6-15

[18] Sun YF, Fujii H, Takaki N, Okitsu Y (2013) Microstructure and mechanical properties of dissimilar Al alloy/steel joints prepared by a flat spot friction stir welding technique. Mater Design 47:350-357

[19] Yin YH, Sun N, North TH, Hu SS (2010) Hook formation and mechanical properties in AZ31 friction stir spot welds. J Mater Process Technol 210:2062-2070

[20] Rosendo T, Parra B, Tier MAD, Silva AAMD, Santos JFD, Strohaecker TR (2011) Mechanical and microstructural investigation of friction spot welded AA6181-T4 aluminium alloy. Mater Design 32(3):1094-1100

[21] Tozaki Y, Uematsu Y, Tokaji K (2010) A newly developed tool without probe for friction stir spot welding and its performance. J Mater Process Tech 210(6):844-851

[22] Chu Q, Yang XW, Li WY, Li YB (2016) Microstructure and mechanical behaviour of pinless friction stir spot welded AA2198 joints. Sci Technol Weld Joi 21:164-170

[23] Li WY, Li JF, Zhang ZH, Gao DL, Wang WB, Dong CL (2014) Improving mechanical properties of pinless friction stir spot welded joints by eliminating hook defect. Mater Design 62:247-254

[24] Suhuddin UFH, Fischer V, Santos JFD (2013) The thermal cycle during the dissimilar friction spot welding of aluminum and magnesium alloy. Scripta Mater 68(1):87-90

[25] Malard B, Geuser FD, Deschamps A (2015) Microstructure distribution in an AA2050-T34 friction stir weld and its evolution during post-welding heat treatment. Acta Mater 101:90-100.

[26] Yamamoto M, Gerlich A, North TH, Shinozaki K (2013) Cracking and local melting in mg-alloy and al-alloy during friction stir spot welding. Weld World 52(9):6406-6413

[27] Solanki KN, Jordon JB, Whittington W, Rao H, Hubbard CR (2012) Structure–property relationships and residual stress quantification of a friction stir spot welded magnesium alloy. Scripta Mater 66(10):797-800

[28] Bozzi S, Helbert-Etter AL, Baudin T, Klosek V, Kerbiguet JG, Criqui B (2010) Influence of FSSW parameters on fracture mechanisms of 5182 aluminium welds. J Mater Process Technol 210(11):1429-1435

Table and figure captions:

Table 1 Chemical composition of AA2198(wt.%).

Table 2 Mechanical properties of AA2198-T8.

Table 3 Process parameters of probeless FSSW.

Fig. 1. Schematic illustration of probeless FSSWed joint.

Fig. 2. Cross-sectional micrographs of probeless FSSWed joint: (a) full view, (b) SZ (region B) and (c) TMAZ and HAZ (region C).

Fig. 3. Schematic illustration of the macrostructure evolution during the probeless FSSW process: (a) rotation, (b) plunge and (c-f) dwell.

Fig. 4. The variations of SW with process parameters: (a) dwell time, (b) plunge rate and (c) rotation speed.

Fig. 5. The variations of SEA and HA with process parameters: (a) dwell time, (b) plunge rate and (c) rotation speed.

Fig. 6. The variations of maximum tensile/shear load and θ with process parameters: (a) dwell time, (b) plunge rate and (c) rotation speed.

Fig. 7. Fracture modes: (a) shear fracture and (b) plug fracture.

Fig. 8. Fractographs of joints: (a) shear fracture and (c) plug fracture.

Table 1 Chemical composition of AA2198 (wt.%).

Cu	Si	Fe	Mg	Zn	Ti	Ag	Zr	Li	Al
2.9-3.5	≤0.08	≤0.1	0.25-0.8	≤0.35	≤0.1	0.1-0.5	0.04-0.18	0.8-1.1	bal

Table 2 Mechanical properties of AA2198-T8.

Yield strength (MPa)	Tensile strength (MPa)	Elongation (%)
469	510	14

Table 3 Process parameters of probeless FSSW.

Parameter	**Value**
Rotation speed (rpm)	600, 750, 950, 1180, 1500
Dwell time (s)	3, 6, 9, 12, 15
Plunge rate (mm/min)	10, 20, 30, 40, 50
Plunge depth (mm)	0.3

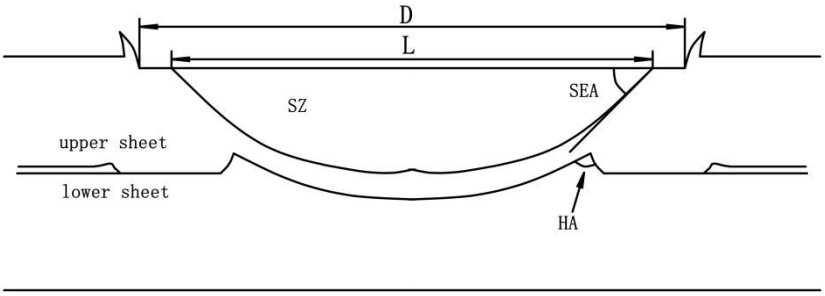

Fig. 1. Schematic illustration of probeless FSSWed joint.

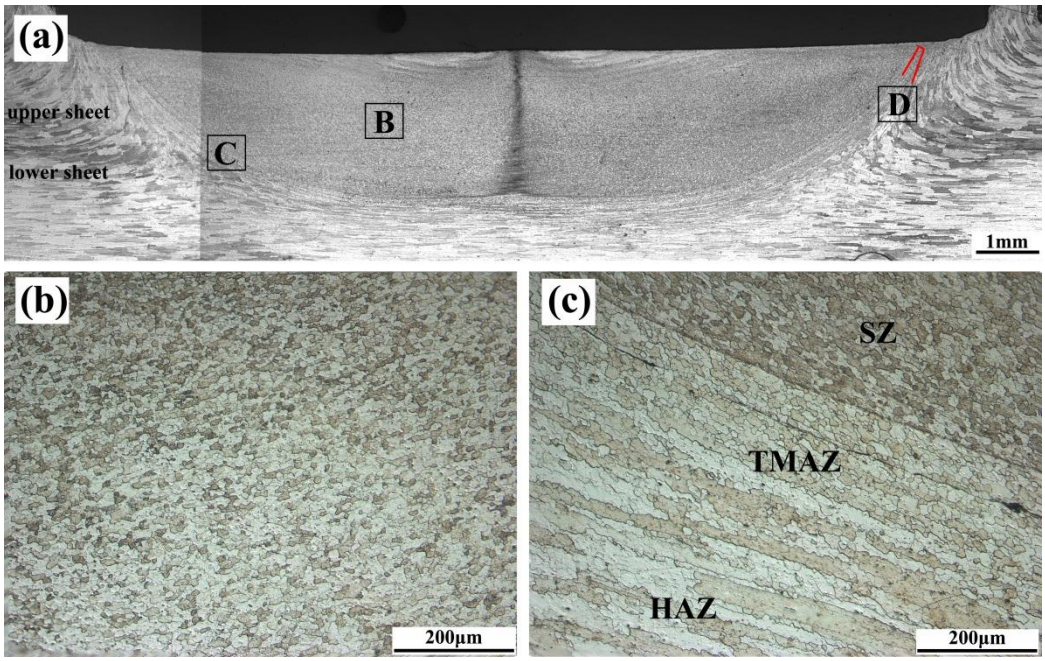

Fig. 2. Cross-sectional micrographs of probeless FSSWed joint:

(a) full view, (b) SZ (region B) and (c) TMAZ and HAZ (region C).

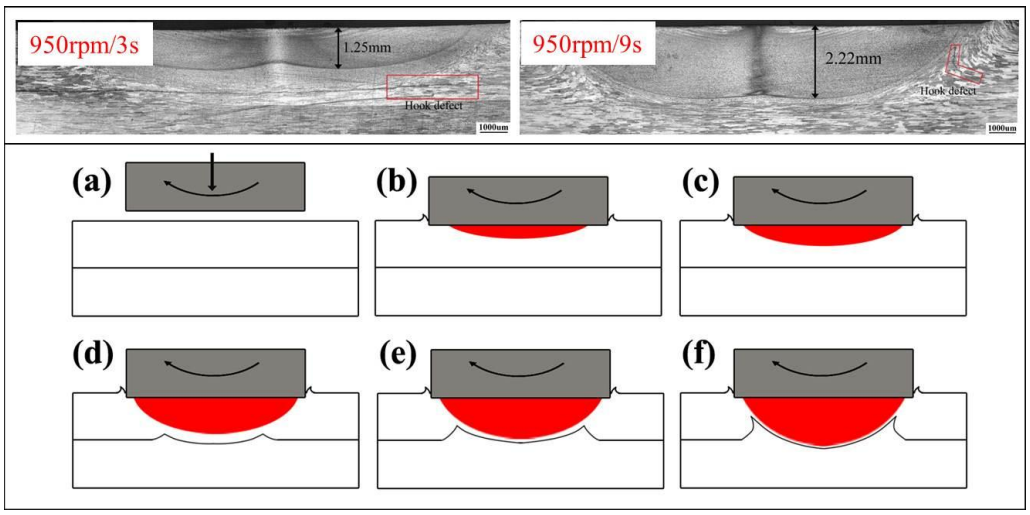

Fig. 3. Schematic illustration of the macrostructure evolution

during the probeless FSSW process: (a) rotation, (b) plunge and (c-f) dwell.

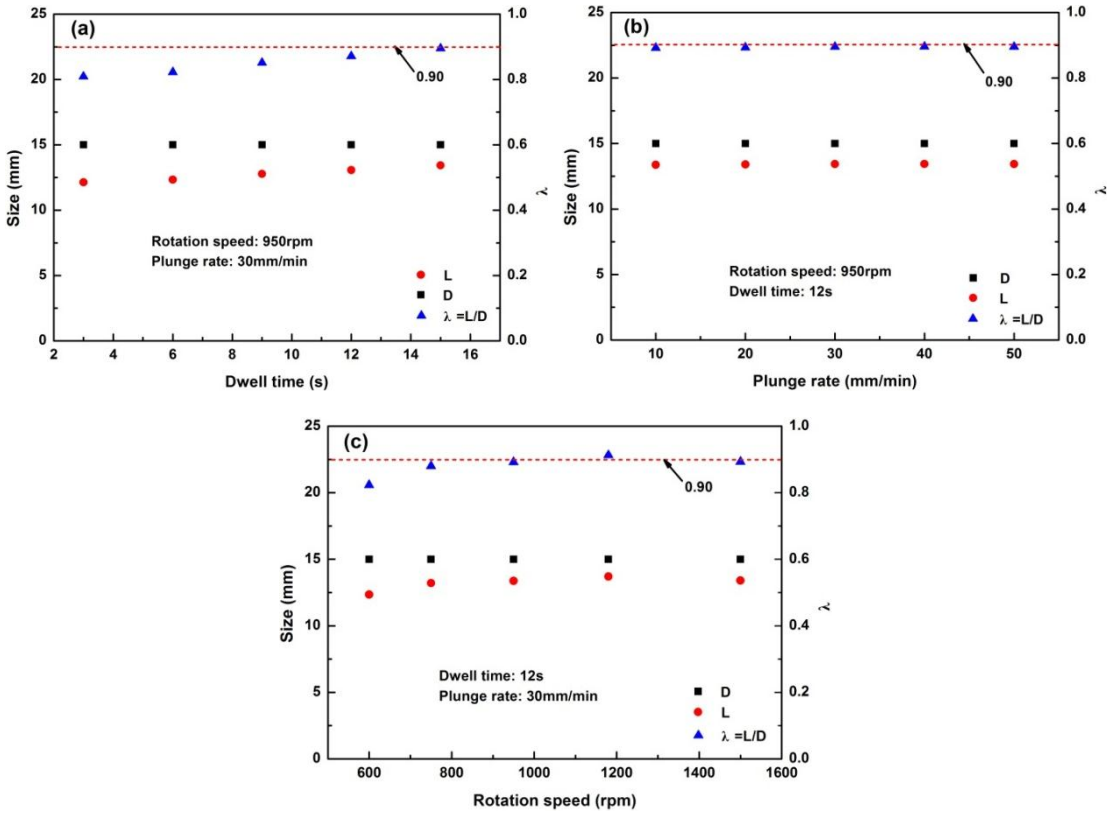

Fig. 4. The variations of SW with process parameters:

(a) dwell time, (b) plunge rate and (c) rotation speed.

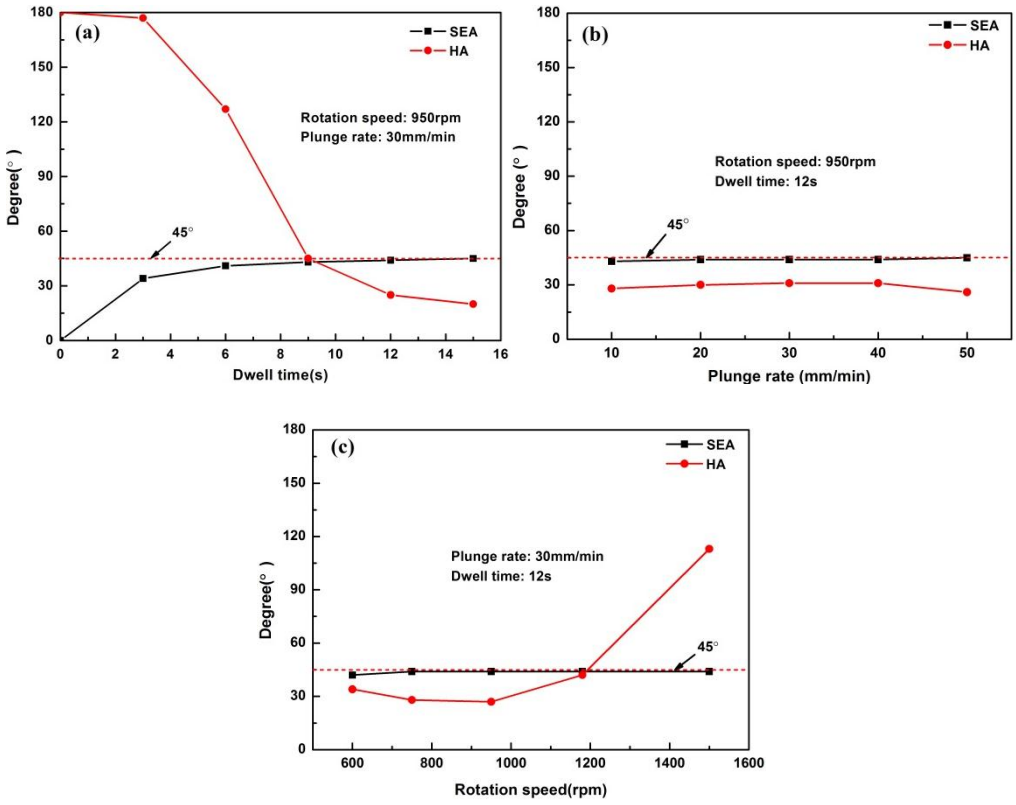

Fig. 5. The variations of SEA and HA with process parameters:

(a) dwell time, (b) plunge rate and (c) rotation speed.

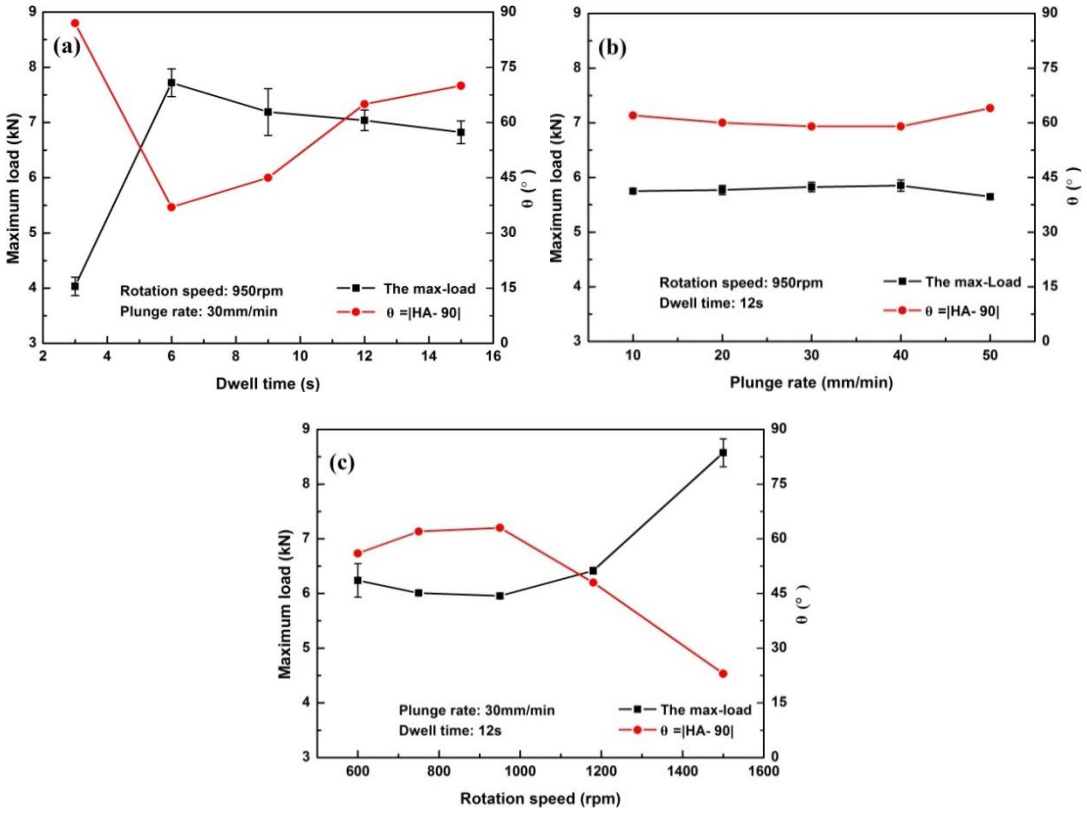

Fig. 6. The variations of maximum tensile/shear load and θ with process parameters:

(a) dwell time, (b) plunge rate and (c) rotation speed.

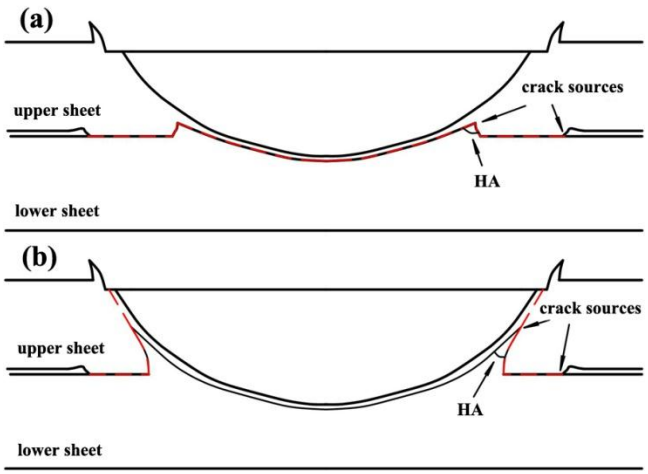

Fig. 7. Fracture modes: (a) shear fracture and (b) plug fracture.

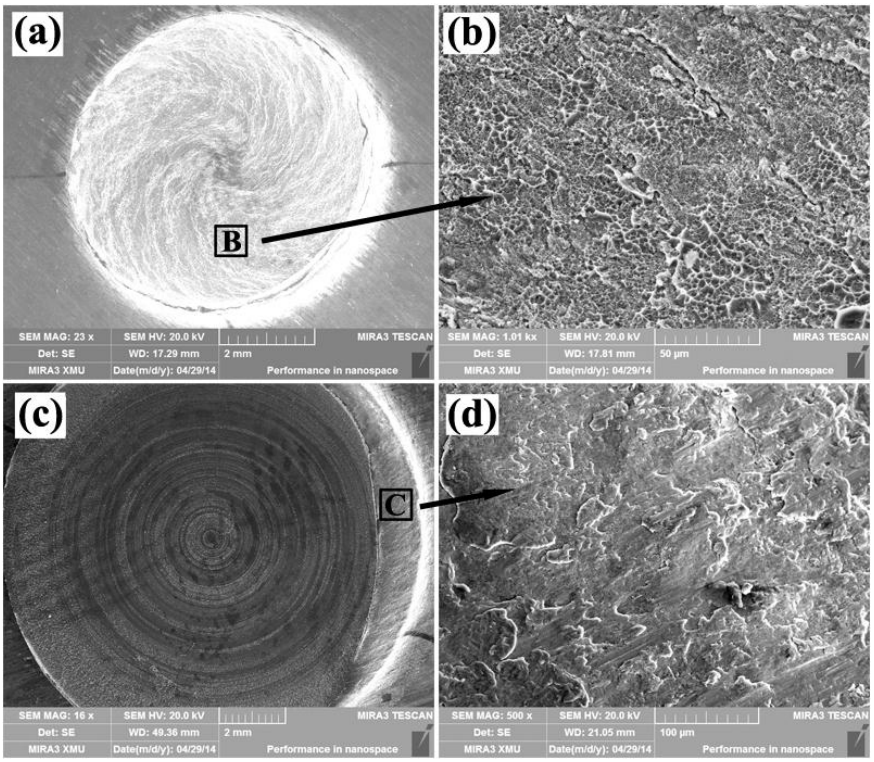

Fig. 8. Fractographs of joints: (a) shear fracture and (c) plug fracture.